A Numerical Model of Viscoelastic Flow in Microchannels

D. Trebotich*, P. Colella†, G. Miller‡ and D. Liepmann††

* Lawrence Livermore National Laboratory
P.O. Box 808, L-560, Livermore, CA, USA, trebotich1@llnl.gov
† Lawrence Berkeley National Laboratory, Berkeley, CA, USA, pcolella@lbl.gov
‡ University of California, Davis, CA, USA, grgmiller@ucdavis.edu
†† University of California, Berkeley, CA, USA, liepmann@me.berkeley.edu

ABSTRACT

We present a numerical method to model non-Newtonian, viscoelastic flow at the microscale. The equations of motion are the incompressible Navier-Stokes equations coupled with the Oldroyd-B constitutive equation. This constitutive equation is chosen to model a Boger fluid which is representative of complex biological solutions exhibiting elastic behavior due to macromolecules in the solution (e.g., DNA solution). Our numerical approach is a projection method to impose the incompressibility constraint and a Lax-Wendroff method to predict velocities and stresses while recovering both viscous and elastic limits. The method is second-order accurate in space and time, free-stream preserving, has a time step constraint determined by the advective CFL condition, and requires the solution of only well-behaved linear systems amenable to the use of fast iterative methods. We demonstrate the method for viscoelastic incompressible flow in simple microchannels (2D) and microducts (3D). [1]

Keywords: non-Newtonian, viscoelasticity, Oldroyd-B, microfluidics, projection methods

1 EQUATIONS OF MOTION

The incompressible Navier-Stokes equations are a combination of evolution equations and constraints due to the incompressibility condition:

$$\begin{aligned} \rho\mathbf{u}_t + \rho\nabla\cdot(\mathbf{u}\otimes\mathbf{u}) &= -\nabla p + \nabla\cdot\bar{\boldsymbol{\tau}} \\ \nabla\cdot\mathbf{u} &= 0 \end{aligned} \qquad (1)$$

where ρ is the fluid density, $\mathbf{u}$ is the velocity of the fluid, p is the isotropic pressure and $\bar{\boldsymbol{\tau}}$ is the shear stress. For Newtonian flow, the shear stress depends on the instantaneous value of the rate of deformation: $\bar{\boldsymbol{\tau}} = 2\mu\mathbf{D}(\mathbf{u})$ with rate of deformation defined as $\mathbf{D}(\mathbf{u}) = \frac{1}{2}(\nabla\mathbf{u}+\nabla\mathbf{u}^T)$. Consequently, incompressible Newtonian flow reduces the Navier-Stokes equations to

$$\rho\mathbf{u}_t + \rho(\mathbf{u}\cdot\nabla)\mathbf{u} = -\nabla p + \mu\Delta\mathbf{u}. \qquad (2)$$

[1]This work was performed under the auspices of the U.S. Department of Energy by the University of California, Lawrence Livermore National Laboratory under contract No. W-7405-Eng-48.

For non-Newtonian, viscoelastic flow of a Boger fluid the shear stress depends on the history of the rate of deformation. The equations of motion are the incompressible Navier-Stokes equations coupled to the Oldroyd-B constitutive equation, an evolution equation for the shear stress contribution due to polymer in the fluid derived from the upper-convected Maxwell equation:

$$\begin{aligned} \rho\mathbf{u}_t + \rho(\mathbf{u}\cdot\nabla)\mathbf{u} &= -\nabla p + \mu_s\Delta\mathbf{u} + \nabla\cdot\boldsymbol{\tau} \\ \boldsymbol{\tau}_t + (\mathbf{u}\cdot\nabla)\boldsymbol{\tau} &= \nabla\mathbf{u}\cdot\boldsymbol{\tau} + \boldsymbol{\tau}\cdot\nabla\mathbf{u}^T \\ &\quad -\frac{1}{\lambda}(\boldsymbol{\tau} - 2\mu_p\mathbf{D}(\mathbf{u})) \end{aligned} \qquad (3)$$

where subscripts s and p refer to solvent and polymer, respectively, and λ is the relaxation time for the polymer. It is helpful to define a dimensionless quantity known as the Deborah number which relates the polymer relaxation to the characteristic flow time: $De = \frac{\lambda}{t} = \lambda\dot{\gamma}$, where $\dot{\gamma} = \sqrt{II}$ and II is a second invariant of the rate of deformation.

These equations demonstrate two interesting limits of the Deborah number: (1) the viscous limit, $De = 0$ ($\lambda = 0$), which yields a Newtonian polymeric stress contribution to the solvent stress in the momentum equation, $\boldsymbol{\tau} = 2\mu_p\Delta\mathbf{u}$; (2) the elastic limit, $De \to \infty$ ($\lambda \to \infty$, μ_p/λ finite). These limits bound the design of the numerical algorithm presented here.

2 NUMERICAL ALGORITHM

The formulation of appropriate time-discretization methods for constrained evolution equations is subtler than evolution equations alone. To address this issue, Chorin [1] introduced projection methods, based on the Hodge decomposition of any vector field into a divergence-free part and a gradient of a scalar field. Projection methods are fractional step methods for which an intermediate velocity is computed that does not necessarily satisfy the incompressibility constraint. Then this velocity is corrected so that it satisfies the constraint. More recently, Bell, Colella, and Glaz (BCG) [2] introduced a predictor-corrector method based on Chorin's ideas. Some of the key advantages of their method are that the advective terms can be treated using explicit high-resolution finite difference methods for hyperbolic partial differential equations (PDE's), and

which are amenable to solution using fast iterative methods such as multigrid, must be solved. This leads to a method that is second-order accurate in space and time. It has a stability constraint on the time step due only to the CFL condition for the advection terms, and a robust treatment of underresolved gradients in the Euler limit. Projection methods have been previously used to study stability of viscoelastic fluids in Taylor-Couette flow [3].

In this section we present a modified version of the BCG algorithm for the case of a time-dependent stress represented by the Oldroyd-B constitutive equation. Our first approach is to treat advective terms with the Lax-Wendroff (LW) method instead of the higher-order Godunov method employed in BCG.

2.1 PROJECTION METHOD WITH REVISED LAX-WENDROFF

Our goal is to design a high-resolution finite difference method to evolve discrete velocity, pressure and stress in time. At the beginning of each timestep, Δt, we know cell-centered grid representations of velocity, pressure and stress: $\mathbf{u}^n_{i,j,k}$, $\nabla p^n_{i,j,k}$, $\boldsymbol{\tau}^n_{i,j,k}$. The following is an algorithm to compute these quantities for discrete timesteps, i.e., to obtain the $t = (n+1)\Delta t$ state, $n = 0, 1, 2, ...$

First, we construct edge-centered velocities via LW, omitting the pressure gradient:

$$\tilde{\mathbf{u}}_{i+\frac{1}{2},j,k} = \frac{1}{2}(\mathbf{u}^n_{i,j,k} + \mathbf{u}^n_{i+1,j,k}) + \frac{\Delta t}{2}(-(\mathbf{u}\cdot\nabla)\mathbf{u} + \frac{\mu_s}{\rho}\Delta\mathbf{u} + \frac{1}{\rho}\nabla\cdot\boldsymbol{\tau})^n_{i+\frac{1}{2},j,k}. \quad (4)$$

The edge velocities are then corrected to account for the pressure (incompressibility) by applying a projection operator:

$$\mathbf{u}^{n+\frac{1}{2}}_{i+\frac{1}{2},j,k} = \tilde{\mathbf{u}}_{i+\frac{1}{2},j,k} - \nabla(\Delta^{-1}(\nabla\cdot\tilde{\mathbf{u}}))_{i+\frac{1}{2},j,k}. \quad (5)$$

We would like to obtain the $t = (n+1)\Delta t$ update to the velocity. In order to do so we first predict a velocity which is not divergence-free by $O(\Delta t^2)$ because of a lagged pressure gradient, and using the midpoint rule for temporal integration:

$$\mathbf{u}^* = \mathbf{u}^n + \Delta t(-[(\mathbf{u}\cdot\nabla)\mathbf{u}]^{n+\frac{1}{2}} - \frac{1}{\rho}\nabla p^{n-\frac{1}{2}} + \frac{\mu_s}{\rho}\Delta(\bar{\mathbf{u}}^{n+\frac{1}{2}}) + \frac{1}{\rho}(\nabla\cdot\boldsymbol{\tau})^{n+\frac{1}{2}}), \quad (6)$$

where $\bar{\mathbf{u}}^{n+\frac{1}{2}} = \frac{1}{2}(\mathbf{u}^n + \mathbf{u}^*)$ approximating Crank-Nicolson and the time-centered advective term is calculated using edge velocities in (5). A final projection operator is applied to the predicted velocity, $\mathbf{u}^*$, enforcing the incompressibility constraint on the velocity and updating the pressure gradient:

$$\mathbf{u}^{n+1} = \mathbf{u}^* - \nabla(\Delta^{-1}(\nabla\cdot\mathbf{u}^*)) \quad (7)$$

$$\nabla p^{n+\frac{1}{2}} = \nabla p^{n-\frac{1}{2}} + \frac{\rho}{\Delta t}\nabla(\Delta^{-1}(\nabla\cdot\mathbf{u}^*)). \quad (8)$$

The stress update follows a similar algorithm. First, we construct a LW stress using only the elastic (hyperbolic) terms:

$$\tilde{\boldsymbol{\tau}}_{i+\frac{1}{2},j,k} = \frac{1}{2}(\boldsymbol{\tau}^n_{i,j,k} + \boldsymbol{\tau}^n_{i+1,j,k}) + \frac{\Delta t}{2}(-(\mathbf{u}\cdot\nabla)\boldsymbol{\tau} + \nabla\mathbf{u}\cdot\boldsymbol{\tau} + \boldsymbol{\tau}\cdot\nabla\mathbf{u}^T)^n_{i+\frac{1}{2},j,k}. \quad (9)$$

We then apply the midpoint rule to account for the viscous terms and predict a time-centered stress:

$$\boldsymbol{\tau}^{n+\frac{1}{2}}_{i+\frac{1}{2},j,k} = \tilde{\boldsymbol{\tau}}_{i+\frac{1}{2},j,k} - \frac{\Delta t}{2\lambda}\left(\boldsymbol{\tau}^{n+\frac{1}{2}}_{i+\frac{1}{2},j,k} - 2\mu_p\mathbf{D}(\bar{\mathbf{u}}^{n+\frac{1}{2}})\right). \quad (10)$$

The stress is then updated to the new time:

$$\boldsymbol{\tau}^{n+1} = \boldsymbol{\tau}^n + \Delta t\left(-(\mathbf{u}\cdot\nabla)\boldsymbol{\tau} + \nabla\mathbf{u}\cdot\boldsymbol{\tau} + \boldsymbol{\tau}\cdot\nabla\mathbf{u}^T\right)^{n+\frac{1}{2}} - \frac{\Delta t}{\lambda}(\boldsymbol{\tau}^{n+1} - 2\mu_p\mathbf{D}(\mathbf{u}^{n+1})). \quad (11)$$

The time-centered stress is used in the velocity predictor (6) to obtain the correct viscous source terms. The viscous operator looks like

$$\mathbf{L}\mathbf{u}^* = \mathbf{u}^n + \Delta t(-[(\mathbf{u}\cdot\nabla)\mathbf{u}]^{n+\frac{1}{2}} - \frac{1}{\rho}\nabla p^{n-\frac{1}{2}} + \frac{1}{2\rho}(\mu_s + \frac{\mu_p\Delta t}{2\lambda+\Delta t})\Delta\mathbf{u}^n + \frac{1}{\rho}\frac{2\lambda}{2\lambda+\Delta t}(\nabla\cdot\tilde{\boldsymbol{\tau}})), \quad (12)$$

where

$$\mathbf{L} = \mathbf{I} - \frac{\Delta t}{2\rho}\left(\mu_s + \frac{\mu_p\Delta t}{2\lambda+\Delta t}\right)\Delta. \quad (13)$$

2.1.1 Viscoelastic Limits

The numerical method captures the appropriate viscous and elastic limits mentioned in Section 1.

Viscous limit. For the Newtonian viscous limit we set $\lambda = 0$ in the algorithm. The time-centered stress reduces to

$$\boldsymbol{\tau}^{n+\frac{1}{2}}_{i+\frac{1}{2},j,k} = 2\mu_p\mathbf{D}(\mathbf{u}^{n+\frac{1}{2}}), \quad (14)$$

and the viscous velocity predictor feels only a Newtonian stress from the polymer in the fluid:

$$\mathbf{u}^* = \mathbf{u}^n + \Delta t(-[(\mathbf{u}\cdot\nabla)\mathbf{u}]^{n+\frac{1}{2}} - \frac{1}{\rho}\nabla p^{n-\frac{1}{2}} + \frac{\mu_s+\mu_p}{\rho}\Delta(\bar{\mathbf{u}}^{n+\frac{1}{2}})). \quad (15)$$

Similarly, the updated stress is

$$\boldsymbol{\tau}^{n+1} = 2\mu_p \mathbf{D}(\mathbf{u}^{n+1}). \tag{16}$$

Elastic limit. For the elastic limit, $\lambda \to \infty$ with μ_p/λ finite, the source term of the stress equation becomes small compared to the upper-convected time derivative and viscous term yielding

$$\boldsymbol{\tau}^{n+\frac{1}{2}}_{i+\frac{1}{2},j,k} = \tilde{\boldsymbol{\tau}}_{i+\frac{1}{2},j,k} + \frac{\Delta t \mu_p}{\lambda}\mathbf{D}(\bar{\mathbf{u}}^{n+\frac{1}{2}}) \tag{17}$$

$$\mathbf{u}^* = \mathbf{u}^n + \Delta t(-[(\mathbf{u}\cdot\nabla)\mathbf{u}]^{n+\frac{1}{2}} - \frac{1}{\rho}\nabla p^{n-\frac{1}{2}} + \frac{\mu_s + \Delta t(\mu_p/\lambda)}{\rho}\Delta(\bar{\mathbf{u}}^{n+\frac{1}{2}})) \tag{18}$$

$$\boldsymbol{\tau}^{n+1} = \boldsymbol{\tau}^n + \Delta t[(-(\mathbf{u}\cdot\nabla)\boldsymbol{\tau} + \nabla\mathbf{u}\cdot\boldsymbol{\tau} + \boldsymbol{\tau}\cdot\nabla\mathbf{u}^T)^{n+\frac{1}{2}} + \frac{2\mu_p}{\lambda}\mathbf{D}(\mathbf{u}^{n+1})]. \tag{19}$$

2.1.2 CFL Condition

The total algorithm is subject to the following restriction on the timestep:

$$\max_{ijk}[|u| + (2(\boldsymbol{\tau}^{xx} + \mu_p/\lambda)/\rho)^{\frac{1}{2}}]\Delta t < \sigma\Delta x, \tag{20}$$

$$\max_{ijk}[|v| + (2(\boldsymbol{\tau}^{yy} + \mu_p/\lambda)/\rho)^{\frac{1}{2}}]\Delta t < \sigma\Delta y, \tag{21}$$

$$\max_{ijk}[|w| + (2(\boldsymbol{\tau}^{zz} + \mu_p/\lambda)/\rho)^{\frac{1}{2}}]\Delta t < \sigma\Delta z, \tag{22}$$

with $\sigma < 1$ for stability and $\boldsymbol{\tau}^{xx}, \boldsymbol{\tau}^{yy}, \boldsymbol{\tau}^{zz} > -\frac{\mu_p}{\lambda}$ which is satisfied automatically by the PDE (3).

2.1.3 Boundary Conditions

The conditions imposed at the boundaries for flow in channels and ducts are (1) solid walls, $\mathbf{u} = 0$, $\frac{\partial\boldsymbol{\tau}}{\partial n} = 0$; (2) inflow, $u = v = 0$, $w = w_{in}$, $\frac{\partial\boldsymbol{\tau}}{\partial n} = 0$; (3) outflow, $\frac{\partial\mathbf{u}}{\partial n} = 0$, $\boldsymbol{\tau} = 0$.

3 RESULTS

We apply our method to flow of a DNA solution in simple (straight, sudden contractions, e.g., Figure 1) microchannels. Experimental data has been used to obtain the rheological parameters specific to this fluid and to also validate the computational model [4]: $\rho = 1$ g/ml, $\lambda = 1.14$ s, $\mu_s = .2538$ g/cm/s and $\mu_p = .02688$ g/cm/s. Channel width is 0.01 cm with a 2:1 contraction ratio. The experimental flow rate is 30μl/hr which corresponds to an average velocity of 0.046 cm/s. These experimental parameters yield $De = 21.1$ and $Re = 0.0016$.

We note some fundamental results (see Table I): (1) the method is free-stream preserving, (2) the method in the Newtonian viscous limit achieves the Newtonian exact solution for 2D steady flow ($\mathbf{u} = (u, w) = (0, w(x))$), and (3) the method in the elastic limit achieves the

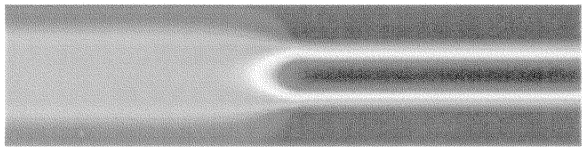

Figure 1: Axial velocity (cm/s) in contracting channel. Flow is left to right. Range: -.007 (blue) to 3.000 (red).

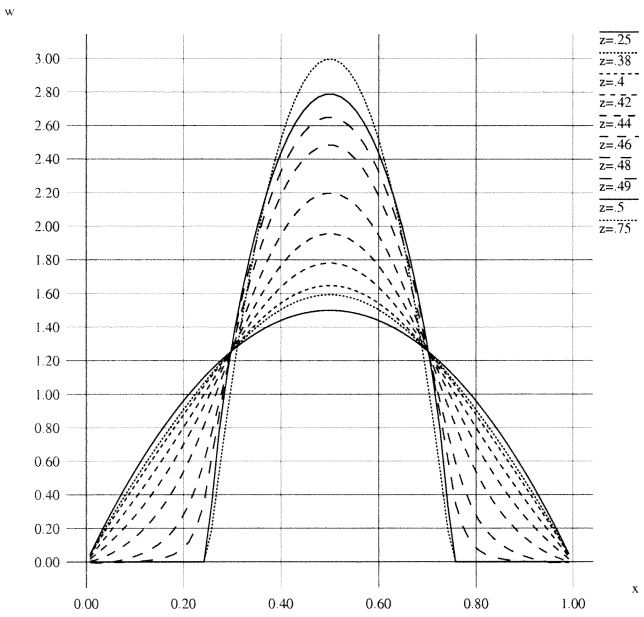

Figure 2: Axial velocity profiles through contracting channel.

Newtonian exact solution of the solvent alone for 2D steady flow. The method calculates a pressure gradient in the viscous limit of -1558.4 g/cm^2/s^2; this matches the Newtonian exact solution of -1559.3 g/cm^2/s^2 for a viscosity $\mu = \mu_s + \mu_p$ and $\frac{dp}{dz} = -\frac{2w_{max}}{\mu R^2}$, where R is half the channel width. The method calculates a pressure gradient in the elastic limit of -1410.0 g/cm^2/s^2; this matches the Newtonian exact solution of -1410 g/cm^2/s^2 for a viscosity $\mu = \mu_s$. The velocity profile is the classic parabolic profile in 2D steady flow: $w = w_{max}[1 - (x - R)^2/R^2]$. The maximum velocity is exactly $w_{max} = \frac{3}{2}w_{avg}$ and calculated as $1.500w_{avg}$. We also note that the velocity profiles in Figure 2 of the 2:1 contracting flow in Figure 1 show maximum velocity of $1.5w_{avg}$ in the first section of the channel and then $3w_{avg}$ in the smaller section which has half the channel width. The negative velocity in the contraction corners indicates flow recirculation.

In Table II we demonstrate second-order accurate convergence rates for the method by estimating error on successively refined grids. The conditions for the convergence study are steady, viscoelastic flow in a straight microchannel.

Table I: Comparison of exact solution to numerical method for 2D steady flow.

	Exact	Method
Pressure gradient in viscous limit	-1559.3	-1558.4
Pressure gradient in elastic limit	-1410	-1408.9
Maximum velocity	1.5	1.500

Table II: Error and convergence rates for viscoelastic flow.

Norm	$e^{1/32}$	Rate	$e^{1/64}$	Rate
L_1	5.86×10^{-3}	2.00	1.46×10^{-3}	2.00
L_2	2.93×10^{-3}	2.00	7.32×10^{-4}	2.00
L_∞	1.47×10^{-3}	1.99	3.70×10^{-4}	1.99
Norm	$e^{1/128}$	Rate	$e^{1/256}$	
L_1	3.66×10^{-4}	2.00	9.16×10^{-5}	
L_2	1.83×10^{-4}	2.00	4.58×10^{-5}	
L_∞	9.31×10^{-5}	2.00	2.33×10^{-5}	

4 CONCLUSIONS

We demonstrate a second-order accurate numerical method for viscoelastic flow in microchannels. The method compares very well to exact solutions for Newtonian viscous fluids in steady flow. In order to properly address the elastic limit in the equations of motion we will modify the scheme, taking advantage of the ability to cast the PDE's (3) in a hybrid conservation form which exploits hyperbolicity while maintaining the viscous and elastic limits. Furthermore, in order to exhibit the full viscoelastic effects (including elastic limit) represented in the Oldroyd-B constitutive equation, we will introduce unsteadiness into the flow by varying the inflow velocity in time or deforming the domain, for example. Finally, we will extend the method to make use of the higher-order Godunov method of the BCG formulation. Higher-order Godunov methods are more robust than LW for hyperbolic systems; steep gradients can be captured while LW tends to smooth discontinuities as seen in compressible flow. Therefore, for certain applications such as sudden contractions and other complex features in microscale geometry it would be advantageous to develop BCG for viscoelasticity.

REFERENCES

[1] Chorin, A. J., *Math. Comp.*, **22**, 745-762, 1968.

[2] J. B. Bell, P. Colella and H. M. Glaz, *J. Comp. Phys.*, **85**, 257-283, 1989.

[3] Kupferman, R., *J. Comp. Phys.*, **147**, 22-59, 1998.

[4] P. Shrewsbury, S. J. Muller and D. Liepmann, *Biomedical Microdevices*, **3**, 225-238, 2001.